Spin and lattice excitations in the heavy-fermion superconductor UNi_2Al_3

B. D. Gaulin,[1,2,5] M. Mao,[1] C. R. Wiebe,[1] Y. Qiu,[3] S. M. Shapiro,[2] C. Broholm,[3,4] S.-H. Lee,[4] and J. D. Garrett[1]
[1]*Department of Physics and Astronomy, McMaster University, Hamilton, Ontario, Canada L8S 4M1*
[2]*Physics Department, Brookhaven National Laboratory, Upton, New York 11973*
[3]*Department of Physics and Astronomy, The Johns Hopkins University, Baltimore, Maryland 21218*
[4]*National Institute of Standards and Technology, Gaithersburg, Maryland 20899*
[5]*Canadian Institute for Advanced Research, 180 Dundas Street W, Toronto, Ontario, Canada M5G 1Z8*
(Received 25 April 2002; published 27 November 2002)

Inelastic neutron scattering measurements have been carried out on the heavy fermion superconductor UNi_2Al_3. This hexagonal material orders magnetically into an incommensurate structure, characterized by the ordering wave vector $\mathbf{Q}_{\rm ord}=(1/2\pm\tau, 0, \frac{1}{2})$ with $\tau\sim 0.11$, below $T_N=4.6$ K and then superconducts below $T_C=1.2$ K. For energies above 2 meV, we observe quasielastic magnetic neutron scattering both near $(0, 0, n/2)$ and in ridges along H of the form $(H, 0, n/2)$, with n odd. This scattering has a characteristic energy width of $\sim$6 meV, and evolves on a temperature scale of $\sim$80 K, which is close to the coherence temperature of this heavy fermion metal. High energy resolution measurements, below 2 meV, show the spectral weight of these fluctuations to evolve from the commensurate wavevector $(0, 0, n/2)$, with n odd, to the material's incommensurate ordering wave vector as the energy of the fluctuations decreases. This observation is particularly interesting in light of the fact that UNi_2Al_3's isostructural sister heavy fermion superconductor, UPd_2Al_3, orders into a commensurate antiferromagnetic structure with this same $(0, 0, n/2)$ wave vector. A search for inelastic magnetic scattering associated with the superconducting phase transition, as has been observed in UPd_2Al_3, revealed no additional scattering at the incommensurate ordering wavevector and energies above 0.10 meV. Measurements of the low-lying acoustic phonons were also performed, and show zone boundary energies lying in the range 10–13 meV.

DOI: 10.1103/PhysRevB.66.174520 PACS number(s): 74.70.Tx, 75.25.+z, 63.20.Dj

INTRODUCTION

The magnetic and superconducting properties of heavy fermion metals have been at the forefront of metals physics research since the discovery of this group of (primarily) uranium and cerium based metals in the late 1970s.[1] Their thermodynamic and transport behavior is clearly exotic, and can be characterized as arising from quasiparticles with very large effective masses; hence their name. However, their ground state properties are also of great interest. The ground state which has attracted the most attention is that in which antiferromagnetism and superconductivity exhibit microscopic coexistence at low temperatures. This occurs for four uranium-based heavy fermion metals: UPt_3,[2–4] URu_2Si_2,[5–7] UPd_2Al_3,[8–11] and UNi_2Al_3.[12–15]

On cooling, all four of these materials undergo phase transitions to an antiferromagnetic state (at $\sim$6 K,[2] 17 K,[5] 14.5 K,[8] and 4.6 K,[12] respectively) before become superconducting (at $\sim$0.5, 1.2, 2.0, and 1.2 K, respectively) at lower temperatures. The ordered moment appearing at the lowest temperatures in UPt_3, URu_2Si_2, and UNi_2Al_3 ($\sim 0.02\mu_B$,[2] $0.04\mu_B$,[6] and $0.21\mu_B$,[9,10] respectively) is sufficiently small to generate speculation[16] that the antiferromagnetic order which they display is either nontrivial, involving multispin rather than dipolar ordering, or parasitic, due to some other symmetry breaking whose origin is as yet unclear. Recent studies appear to eliminate the possibility of non-dipole ordering, at least in URu_2Si_2.[17] However, one recent Si NMR study[18] suggested spatially inhomogeneous antiferromagnetism in URu_2Si_2 under pressure, while a second[19] suggests the presence of an additional order parameter beyond the previously detected spin order.[6,17]

These antiferromagnetic heavy fermion superconductors possess, in fact, three relevant temperature scales. In addition to T_N and T_C, they display a coherence temperature which separates a high temperature regime in which they are relatively poor metals and have resistivities which are only weakly temperature dependent, sometimes characteristic of a semiconductor, from a low temperature regime in which their resistivity rapidly decreases with decreasing temperature. In the case of UNi_2Al_3, the subject of the present study, the coherence temperature is roughly 80 K.[15]

Superconductivity and antiferromagnetism in UPd_2Al_3 (Ref. 8) and UNi_2Al_3 (Ref. 12) were discovered only relatively recently. The literature for UPd_2Al_3 is much more extensive than that which exists for UNi_2Al_3, as single crystals of UNi_2Al_3 have been much harder to grow. Both ternary metals crystallize into the $P6/mmm$ hexagonal space group and the uranium atoms lie on a simple hexagonal lattice. Neutron scattering measurements on UPd_2Al_3 (Refs. 9 and 10) show that it orders into a simple, $\mathbf{Q}=(0, 0, \frac{1}{2})$ antiferromagnetic structure in which the moments lie within the basal plane in ferromagnetic sheets that are antiparallel to those in adjacent basal planes. All measurements[9–11] show a substantial ordered moment at low temperatures, $\sim 0.85\mu_B$ per U atom. This value is much larger than that in UPt_3 or URu_2Si_2, but still much reduced compared with the effective moment of $3.2\mu_B$ per U atom derived from high temperature susceptibility data.[8] Previous elastic neutron scattering measurements[13,14] on a single crystal of UNi_2Al_3 show that,

below $T_N = 4.6$ K, it orders into an incommensurate antiferromagnetic state characterized by the $\mathbf{Q}_{\text{ord}} = (\frac{1}{2} \pm \tau, 0, \frac{1}{2})$ with $\tau \sim 0.11$, ordering wave vector. These results show the magnetic structure to be described by an almost longitudinal spin density wave, wherein the moments lie along nearest-neighbor **a** directions in the basal plane, and are modulated in magnitude from site to site, with a maximum amplitude of $(0.21 \pm 0.1)\mu_B$. This long range order is well described as being due to the $5f$ electrons on the uranium site with no evidence of magnetism associated with the nickel site.

In this paper we report on inelastic neutron scattering results, primarily on the spin dynamics of UNi_2Al_3. The spin excitations in the other three uranium-based heavy fermion superconductors have been rather extensively studied by neutron scattering techniques. Both UPd_2Al_3 (Ref. 9) and URu_2Si_2 (Ref. 6) show well defined spin wave excitations, at least below T_N, and in that sense they are quite conventional. In the case of URu_2Si_2,[6] the spin excitation spectrum is gapped, and longitudinal in polarization, consistent with the spins being polarized along the unique **c** axis in this body-centered-tetragonal material. The spin excitations are heavily damped for wave vectors with a significant component along **c***, even at the lowest temperatures, and spin waves at all wave vectors broaden quickly for temperatures near to and above T_N. As already mentioned the spins in the ordered state of UPd_2Al_3 lie within the hexagonal basal plane, and the spin wave spectrum is gapless. Recent measurements[22,23] on spin excitations in UPd_2Al_3 showed pronounced effects on this spectrum on entering the superconducting phase, below $T_C \sim 2$ K, indicating a fundamental role for the spin fluctuations in mediating the superconducting state.

The spin excitation spectrum in UPt_3 is quite different to that described for UPd_2Al_3 and URu_2Si_2. No propagating spin wave excitations exist at any wave vector, although a quasielastic continuum of scattering with a characteristic energy width of ~ 5 meV is observed, which is maximum at wave vectors such as (0, 0, 1) corresponding to antiferromagnetic correlations between hexagonal closed packed basal planes. The temperature dependence of this scattering is such that all wave vector dependence is gone by ~ 30 K, which corresponds roughly to its coherence temperature.[2]

A comparison between UNi_2Al_3 and UPd_2Al_3 is particularly interesting as these two systems are both isostructural and quasi-isoelectronic. Palladium sits directly below nickel in the periodic table. The conduction electron density in UPd_2Al_3 should be slightly lower than that in UNi_2Al_3, as the UPd_2Al_3 displays hexagonal a and c lattice parameters that are $\sim 4\%$ and $\sim 3\%$ larger than those which UNi_2Al_3 displays.

The heavy fermion state[20] is often described as being related to a lattice Kondo problem in which the competing tendencies of the conduction electrons to screen out local magnetic moments at the uranium site is balanced by the tendency of the conduction electrons to be polarized by the local moments and to mediate RKKY interactions, thereby enhancing the local moments. Both of these tendencies are increasing functions of the density of quasiparticle states at the Fermi energy, $g(\epsilon_F)$, and hence the density of quasiparticles, but they are quite different functions of $g(\epsilon_F)$. At low values of $g(\epsilon_F)$ the tendency to RKKY interactions wins out, and an ordered magnetic state is stabilized. Such a picture is fully consistent with the antiferromagnetic structures displayed by UNi_2Al_3 and UPd_2Al_3, in which a conventional state with relatively large local moments is present at low temperatures for the lower electron density compound UPd_2Al_3.

While the larger ordered moments in UPd_2Al_3 are consistent with this picture, the very different ordered structures, one commensurate with the lattice and the other incommensurate, remains quite mysterious for two metallic compounds which, otherwise, have so much in common. In this paper we will describe inelastic neutron scattering measurements which show the spin fluctuations do indeed have much in common in the two materials. The differences between the magnetism in the two occurs on energy scales less than $T_N \sim 4.6$ K for UNi_2Al_3; for energies beyond $\sim T_N$, the spectral weight for the fluctuations in UNi_2Al_3 moves clearly to the commensurate wave vector at which UPd_2Al_3 orders.

EXPERIMENTAL DETAILS

Measurements were carried out at the High Flux Beam Reactor of Brookhaven National Laboratory (BNL) in four separate experiments using two different triple-axis spectrometers, and at the research reactor of the National Institute for Standards and Technology (NIST) using the SPINS cold neutron triple axis spectrometer. All measurements were performed with pyrolytic graphite (0, 0, 2) serving as both monochromator and analyzer. Although there are differences in the four BNL configurations, the energy resolution in all four experiments was similar, ~ 1.5 meV [full width at half maximum (FWHM)].

The experiments on SPINS at NIST used low energy neutrons from a cold neutron guide, and a novel multi-crystal analyzer. These measurements employed only geometrical collimation to take advantage of the focussing analyzer at the SPINS beamline. The energy resolution was improved to 0.15 and 0.10 meV (FWHM), depending on whether final neutron energies of 3.7 or 2.5 meV were used, respectively.

The experiments were performed on the same high quality single crystal sample[13,14] of UNi_2Al_3 used in prior elastic neutron scattering studies. This crystal was comprised of three large closely aligned grains, having a total mosaic spread of 1.5°. As already described this crystal displays the simple hexagonal crystal structure and lattice parameters at 4.2 K of $a = 5.204$ Å and $c = 4.018$ Å. In order to access a wide range of temperatures from above the coherence temperature ~ 80 K, to below $T_C \sim 1.2$ K, conventional flow cryostats, a ^{3}He cryostat with a 6-T vertical magnetic field, as well as a dilution refridgerator, were employed. In all the experiments, the crystal was mounted in a helium exchange gas with its $(H, 0, L)$ plane coincident with the scattering plane, thus allowing access to the ordering wave vector.

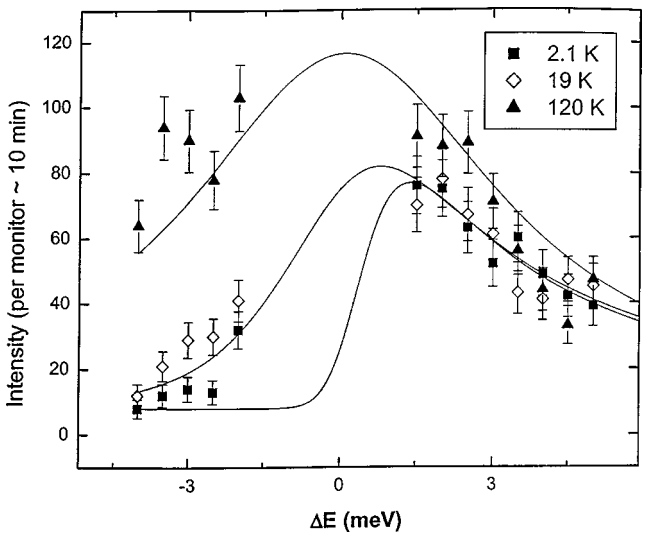

FIG. 1. Constant-$\mathbf{k}_i$ measurements, at the antiferromagnetic ordering wave vector (0.61, 0, 0.5), are shown for three temperatures, one below and two well above T_N. These data clearly show thermally activated inelastic scattering on the neutron energy gain side (negative energies), while the scattering on the neutron energy loss side is essentially temperature independent between 2 K and at least 120 K. The solid lines are fits as described in the text.

LOW RESOLUTION QUASIELASTIC MAGNETIC SCATTERING AT LOW TEMPERATURES

Initial measurements were made in which the inelastic scattering spectrum was examined around the incommensurate antiferromagnetic ordering wave vector. These measurements were made in constant-$\mathbf{k}_i$ geometry, and are shown in Fig. 1. Constant-$\mathbf{Q}=(0.61, 0, \frac{1}{2})$ energy scans were taken at temperatures of 2, 19, and 120 K. They clearly show a dramatic rise in the inelastic intensity on the neutron energy gain side of the scan (negative energies), while the intensity on the neutron energy loss side (positive energies) is roughly temperature independent over this range of temperatures. This identifies the low energy (less than 5 meV) component of the scattering as arising from inelastic fluctuations, as opposed to background as one may have concluded from observation of the neutron energy loss side alone. There was no evidence for propagating magnetic modes, such as spin waves, which would be identified as inelastic peaks in the spectra. The dynamic structure factor for neutron scattering can be written as

$$S(\mathbf{Q},\hbar\omega)=\frac{1}{\pi}\left[1-\exp\left(-\frac{\hbar\omega}{k_BT}\right)\right]^{-1}\mathrm{Im}\,\chi(\mathbf{Q},\hbar\omega). \quad (1)$$

The relative temperature independence of the inelastic scattering in neutron energy loss shown in Fig. 1 is rather remarkable as it implies that the temperature dependence of the imaginary part of the dynamic susceptibility, $\mathrm{Im}\,\chi(\mathbf{Q},\hbar\omega)$ compensates for the temperature dependence of the Bose population factor, over a range of $\hbar\omega/k_BT$ from $\sim$0.14 to 27.5. The lines drawn in Fig. 1 are fits of the data to Eq. (1) with

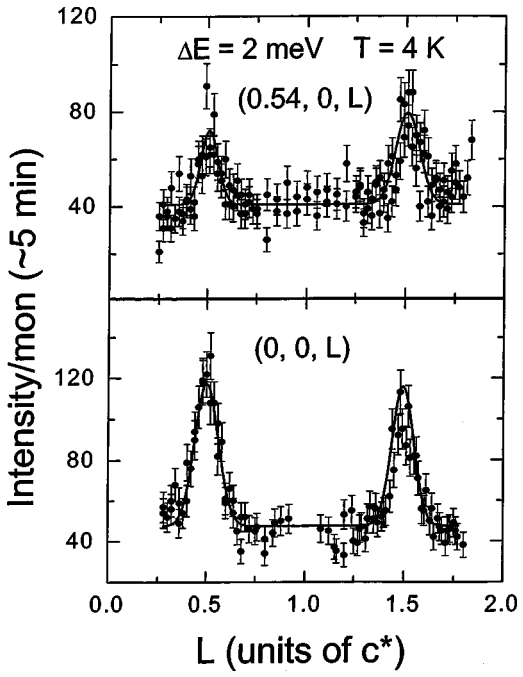

FIG. 2. Constant energy transfer $\Delta E=2$ meV measurements at $T=4$ K of the form (0.54, 0, L) (top) and (0, 0, L) (bottom) are shown. These measurements show the Q dependence of the quasielastic scattering, which is composed of diffuse scattering at (0, 0, $\frac{1}{2}$) and equivalent wave vectors as well as in ridges along (H, 0, $\frac{1}{2}$) and equivalent wave vectors. The solid lines are Lorentzian fits to the peaks intended as guides to the eye.

$$Im\,\chi(\mathbf{Q},\hbar\omega)=\frac{\chi_0\Gamma\hbar\omega}{((\hbar\omega)^2+\Gamma^2)}, \quad (2)$$

and $\Gamma=1.5$, 2.5, and 3.8 meV for 2, 19, and 120 K, respectively. These fits assume a constant background, and have been corrected for the varying analyzer sensitivity, which goes as $k_F^3\cot(\theta_A)$.

Constant-energy scans were performed with the energy transfer set at 2 and 5 meV with the purpose of investigating the **Q** dependence of the quasielastic scattering shown in Fig. 1. These, and all subsequent measurements, were performed in a constant-$\mathbf{k}_f$ geometry. What was found was both interesting and unexpected. Representative constant energy scans at 2-meV energy transfer and 4 K are shown in the two panels that make up Fig. 2. The bottom panel shows a scan along $(0,0,L)$ and clear peaks are seen in this quasielastic scattering at $(0,0,n/2)$ with n odd. Scans were also made through the peak at (0, 0, $\frac{1}{2}$), but in the perpendicular direction, along H in scans of the form $(H,0,\frac{1}{2})$. Together these scans show that there is a relatively well-localized distribution of quasielastic scattering around (0, 0, $\frac{1}{2}$). Other measurements show similar distributions of quasielastic scattering around (0, 0, $\frac{3}{2}$) and (0, 0, $\frac{5}{2}$).

However, scans of the form $(0.54,0,L)$, as shown in the top panel of Fig. 2, reveal another source of quasielastic scattering which extends out in H, as a ridge of scattering along $(H,0,n/2)$ with n odd. This scattering is weaker than that observed at $(0,0,n/2)$, but is still clearly observed

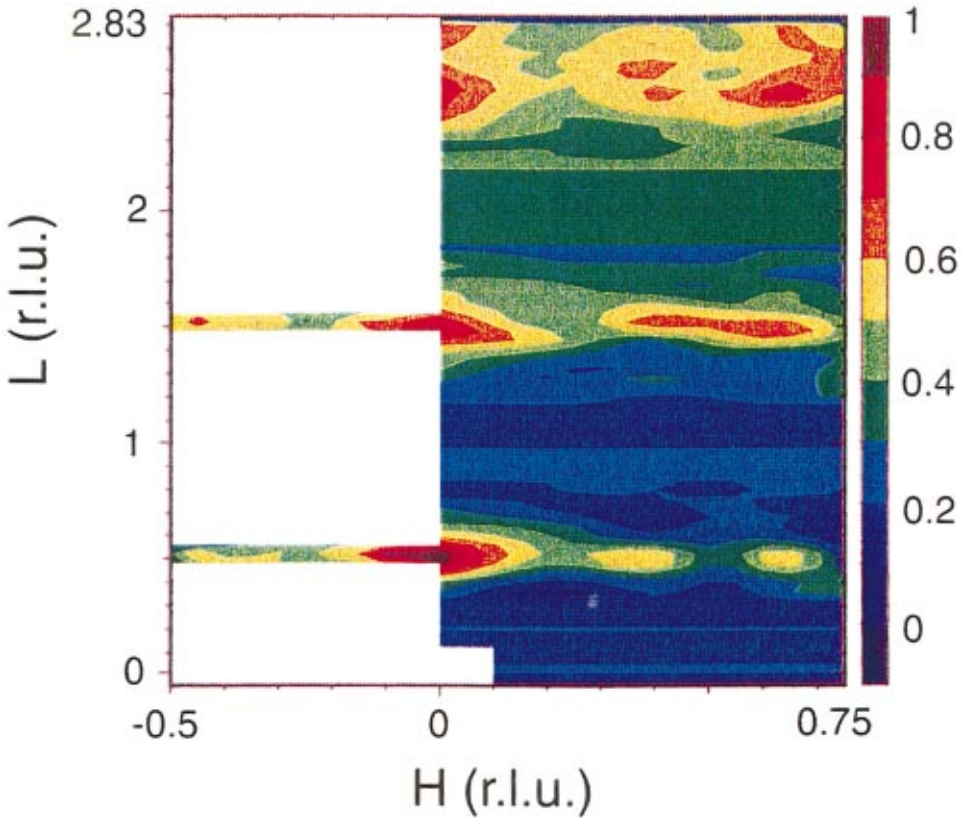

FIG. 3. (Color) A color contour map of the inelastic scattering with $\Delta E = 2$ meV taken at 2 K. The inelastic features at $(0, 0, \frac{1}{2})$ and equivalent wave vectors as well as in ridges along $(H, 0, \frac{1}{2})$ and equivalent wave vectors are evident. This map was constructed using scans of the form $(H_0, 0, L)$ with seven different values of H_0, and of the form $(H, 0, L)$ with $L = \frac{1}{2}$ and $\frac{3}{2}$.

above background. All of the scattering observed, except for that precisely at the magnetic ordering wavevector, $\mathbf{Q}_{\text{ord}} = (\frac{1}{2} \pm \tau, 0, \frac{1}{2})$, was inelastic in origin. Elastic scattering scans carried out with pyrolitic graphite filters in both incident and scattered beams to reduce the possibility of higher order contamination, showed no intensity above background either at $(0, 0, n/2)$ with n odd, or along H in scans of the form $(H, 0, n/2)$, with the aforementioned exception of precisely at the ordering wavevectors, $H = 0.39$ and 0.61. Elastic scans made on the SPINS cold neutron triple axis spectrometer also bear this out at high energy resolution (that is with the elastic scattering condition enforced at a higher tolerance). This data will be discussed later.

Constant-energy measurements of the form $(H_0, 0, L)$ with the energy transfer set at 2 and 5 meV were carried out for seven different values of H_0, between 0 and 1.0, as well as scans of the form $(H, 0, n/2)$ with $n = \frac{1}{2}$ and $\frac{3}{2}$, all at a temperature of 2 K. These were combined so as to form a contour map of this quasielastic scattering. The data is qualitatively similar at 2 and 5 meV, but the scattering is stronger at 2 meV. The resulting contour map derived from the 2-meV data is shown in Fig. 3. One can clearly see both the localized scattering around $(0, 0, n/2)$ with n odd, and that which extends out along $(H, 0, n/2)$ with n odd. The scattering at $(0, 0, n/2)$ is identified as magnetic, as it clearly decreases in intensity as n increases. The magnetic neutron scattering cross section is sensitive to only those components of moment which lie in a plane perpendicular to $\mathbf{Q}$. These are the same for all values of n at $(0, 0, n/2)$, so its only expected n dependence is that of the magnetic form factor, which falls off for increasing $|\mathbf{Q}|$.

The scattering which extends out along $(H, 0, n/2)$ is more difficult to be definitive about. The relationship between $\mathbf{Q}$ and the crystallographic lattice is more complicated, and this makes the identification of its nature more difficult. It is made more difficult still by interference with a multiphonon background, which is a strongly increasing function of $|\mathbf{Q}|$. However, as will be discussed later, on lower energy scales, accessible in cold neutron experiments, and at temperatures of the order of T_N and below, this band of scattering develops structure as a function of H, peaking up near the ordering wavevectors at H = 0.39 and 0.61. Thus we conclude that this scattering is also magnetic in origin.

Constant-$\mathbf{Q}$ measurements were carried out in constant-$\mathbf{k}_f$ mode both using a scattered energy of 14.7 meV, and using a scattered energy of 30.5 meV. They were made at a variety of wavevectors, chosen once the systematic $\mathbf{Q}$ behavior of this scattering was well understood, as discussed above. Figure 4 shows measurements made at $\mathbf{Q} = (0, 0, 0.5)$ and (0, 0, 2.5), as well as at (0, 0, 0.75), which acts as a measure of the background (see Fig. 3). These measurements show that the quasielastic scattering at 2 K is characterized by an approximate energy scale of 6 meV. Similar measurements at $\mathbf{Q} = (0.54, 0, \frac{1}{2})$ lead to the same conclusion with regard to the energy scale of the ridge of scattering along $(H, 0, n/2)$ with n odd.

TEMPERATURE DEPENDENCE OF THE QUASIELASTIC SCATTERING

On warming the sample from 2 K, relatively minor changes occur in the form of the quasielastic scattering, until

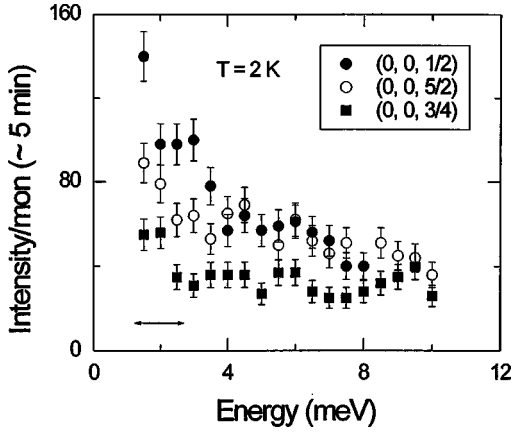

FIG. 4. Constant-**Q** inelastic scans at $T=2$ K are shown. These scans are taken with **Q** along the same direction, (0, 0, L), at $(0, 0, n/2)$, with n odd. The scattering at $(0, 0, \frac{3}{4})$ is representative of background at this low temperature. The horizontal bar gives the energy resolution of the measurement, ~1.5 meV (FWHM).

temperatures of the order of the coherence temperature (~80 K) are reached. Representative scans at 25 and 100 K along $(0, 0, L)$ at an energy transfer of 2 meV are shown in the bottom panel of Fig. 5, while scans along $(0.54, 0, L)$ are shown in the top panel of Fig. 5. It is evident from both of these panels that the form of this scattering at 25 K is more or less identical to that at much lower temperatures (see Fig. 2) and that the characteristic temperature scale for the evolution of the **Q** dependence of this scattering is high, ~80 K. It is also evident that the **Q** structure goes away at higher temperatures, not by having the maxima diminish in intensity and dissolve into the background, but rather by having the background rise up to envelop the low temperature **Q** dependence.

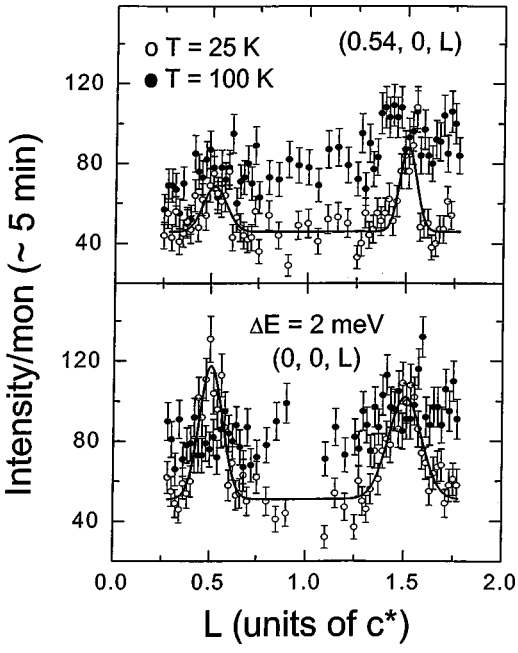

FIG. 5. Constant energy transfer $\Delta E=2$ meV measurements at $T=25$ and 100 K, are shown. The top panel shows scans of the form (0.54, 0, L), while the bottom panel shows (0, 0, L) data. It is evident that most of the thermal evolution of the scattering occurs above 25 K, and that this behavior is quite different along (0.54, 0, L) compared with (0, 0, L). As in Fig. 3, the solid lines are Lorentzian fits to the peaks in the 25-K data sets, intended as guides to the eye.

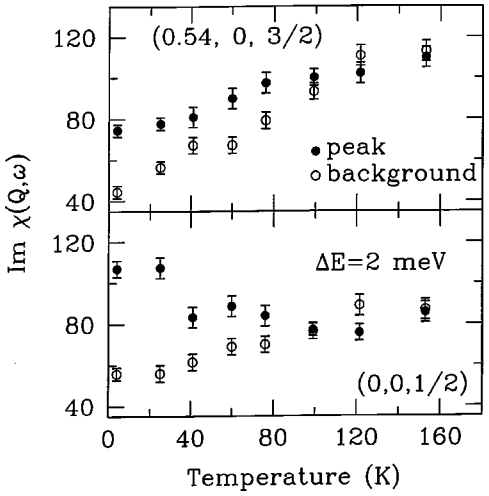

FIG. 6. The temperature dependence of Im $\chi(\mathbf{Q},\hbar\omega=2$ meV) derived from a constant energy transfer $\Delta E=2$ meV measurements taken near the peak along L in data at (0.54, 0, $\frac{3}{2}$) and (0, 0, $\frac{1}{2}$) is shown along with that to either side of these peaks along L, the background. Two things are immediately evident: this inelastic scattering evolves on a temperature scale which is ~100 K, and the form of the evolution of this scattering is quite different in the vicinity of these two wave vectors.

The form of this thermal evolution is most clearly shown in Fig. 6, wherein Im $\chi(\mathbf{Q},\hbar\omega)$, the imaginary part of the dynamic susceptibility, at $\hbar\omega=2$ meV is displayed as a function of temperature for several important wave vectors. These are both maxima and minima of the scattering. The wave vectors are (0, 0, $\frac{1}{2}$) (a maximum, ''peak''), (0, 0, $\frac{3}{4}$) (a minimum, ''background''); as well as (0.54, 0, $\frac{1}{2}$) (a maximum, ''peak'') and (0.54, 0, $\frac{3}{4}$) (a minimum, ''background''). Im $\chi(\mathbf{Q},\hbar\omega)$ is related to the scattering through the Bose temperature factor, as shown in Eq. (1). Clearly, the **Q** structure of this quasielastic scattering is largely gone by ~80 K.

QUASIELASTIC SCATTERING WITHIN THE SUPERCONDUCTING STATE

Measurements were also performed at low temperatures and relatively high magnetic fields, in order to probe the behavior of these fluctuations as the superconducting phase is entered below $T_C\sim1.2$ K. These measurements are shown in the top panel of Fig. 7 for scans along $(0, 0, L)$ and in the bottom panel of Fig. 7 for scans along $(0.54, 0, L)$. As can be seen, all of these measurements show that there is no change in this quasielastic scattering, at least not at energies above ~1.5 meV, as the superconducting phase is entered, or as a function of applied magnetic field. This seems to be reasonable, as the energy scale for these fluctuations, ~6 meV ~70 K, far exceeds that of $T_C\sim1.2$ K, or, for that matter $T_N\sim4.6$ K. In addition the lack of a field dependence is un-

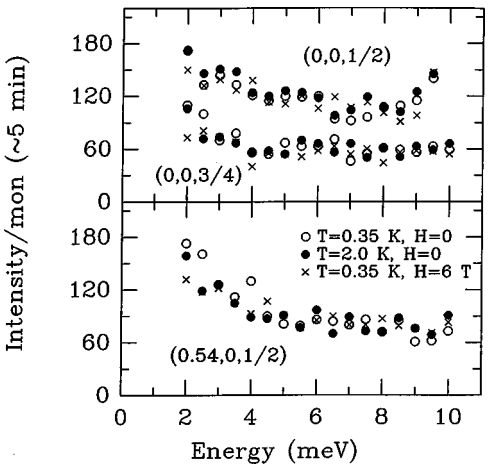

FIG. 7. Constant-**Q** inelastic scans near and below the onset of superconductivity at $T_C = 1.2$ K. The top panel shows data taken at (0, 0, $\frac{1}{2}$), as well as expected background data at (0, 0, $\frac{3}{4}$), at temperatures above and below superconducting $T_C \sim 1.2$ K, and in the presence of a 6-T magnetic field directed along an (h, h, 0) direction. The bottom panel shows similar data at (0.54, 0, $\frac{1}{2}$). This data clearly indicate that this inelastic scattering is oblivious to the presence of the superconducting state.

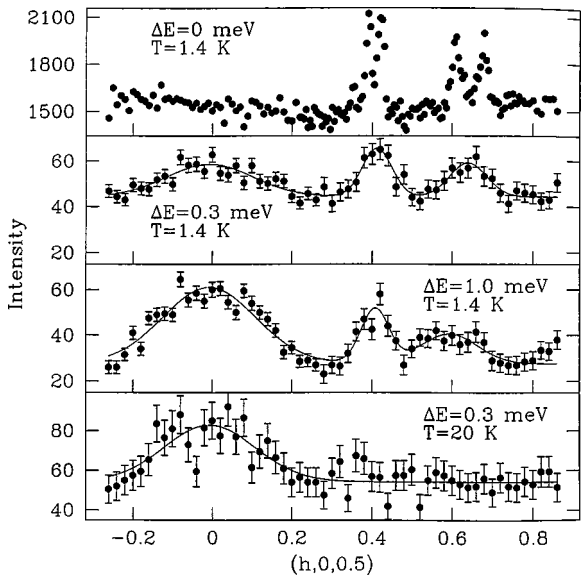

FIG. 8. High resolution, constant energy transfer scans taken with the SPINS spectrometer at NIST are shown. The top panel shows elastic scattering at $T = 1.4$ K, clearly showing the incommensurate magnetic Bragg peaks at (0.39, 0, $\frac{1}{2}$) and (0.61, 0, $\frac{1}{2}$). The second and third panels from the top show constant ΔE scans at $\Delta E = 0.3$ and 1.0 meV, respectively, also at $T = 1.4$ K. Clearly the scattering shifts from the incommensurate ordering wave vectors to the (0, 0, $\frac{1}{2}$) commensurate position as the energy transfer increases. The bottom panel shows low energy transfer constant $\Delta E = 0.3$ meV data, but at $T = 20$ K, well above $T_N = 4.6$ K. Little, if any, spectral weight is present at the incommensurate ordering wave vectors, while that at the commensurate (0, 0, $\frac{1}{2}$) position remains relatively strong.

surprising, despite the strong field dependence for vertical magnetic fields on the superlattice intensity of the incommensurate magnetic long range order.[14,15] This quasielastic scattering is clearly connected with the third temperature scale relevant to this material, the coherence temperature ~80 K, and appears to be unrelated to the magnetic long range order which sets in below 4.6 K.

HIGH RESOLUTION QUASIELASTIC MAGNETIC SCATTERING

Constant energy scans at very low energy transfers ($\hbar\omega = 0$ and 0.3 meV as well as at $\hbar\omega = 1.0$ meV) were performed using the SPINS triple axis spectrometer located on a cold neutron guide at NIST. These relatively high energy resolution measurements allowed us to probe the quasielastic magnetic response on an energy scale relevant to T_N.

High resolution constant-E scans in H of the form (H, 0, 0.5) are shown in Fig. 8. These scans pass through the incommensurate ordering wavevectors at (0.5 $\pm\tau$, 0, 0.5), as well as the commensurate wavevector (0, 0, 0.5) at which UPd_2Al_3 orders. The top three panels of Fig. 8 show data taken at 1.4 K, well below T_N, but just above T_C, while the bottom panel is at 20 K, well above T_N and T_C, but well below the coherence temperature.

The top panel shows elastic scattering and magnetic Bragg peaks are clearly seen at (0.5 $\pm\tau$, 0, 0.5), with $\tau = 0.11$. The splitting seen in the Bragg peaks is due to the crystal mosaic, however it is clear that all the elastic intensity is located at the incommensurate ordering wavevectors. The middle two panels show constant-E scans at 0.3 meV energy transfer and 1.0-meV energy transfer. Clearly a broad magnetic peak develops in the inelastic scattering at (0, 0, 0.5) and becomes stronger as the energy transfer progressively becomes greater. That is, the spectral weight of the magnetic inelastic scattering moves from the incommensurate ordering wavevectors, (0.5 $\pm\tau$, 0, 0.5), with $\tau = 0.11$, to the commensurate wave vector which describes the Neel state in UPd_2Al_3, as the characteristic energy scale of the fluctuations increases. Above T_N, as seen in the bottom panel of Fig. 8, little magnetic inelastic scattering remains at the incommensurate wave vectors; the spectral weight of the inelastic scattering is decidely associated with wave vector describing the simple antiferromagnetic stacking of ferromagnetic sheets which is the Neel state displayed by UPd_2Al_3.

While it is not obvious from the high energy resolution measurements shown in Figs. 8 and 9, the inelastic scattering at and near the the incommensurate ordering wave vectors, (0.5 $\pm\tau$, 0, 0.5), with $\tau = 0.11$ extends out to energies of ~6 meV. This was shown in Figs. 1–3. The top panel of Fig. 6 shows that the **Q** dependence of this quasi-elastic scattering only disappears on the temperature scale of the coherence temperature, ~80 K, as does the quasielastic scattering at the commensurate wave vector which describes the Neel state in UPd_2Al_3, (0, 0, 0.5), whose temperature dependence was shown in the bottom panel of Fig. 6.

The top panel of Fig. 9 shows Im $\chi(\mathbf{Q},\hbar\omega)$ extracted from high resolution, constant-**Q** scans at 1.4 K, at both the commensurate wave vector (0, 0, 0.5) and one of the incommensurate ordering wave vectors (0.39, 0, 0.5). The subtraction

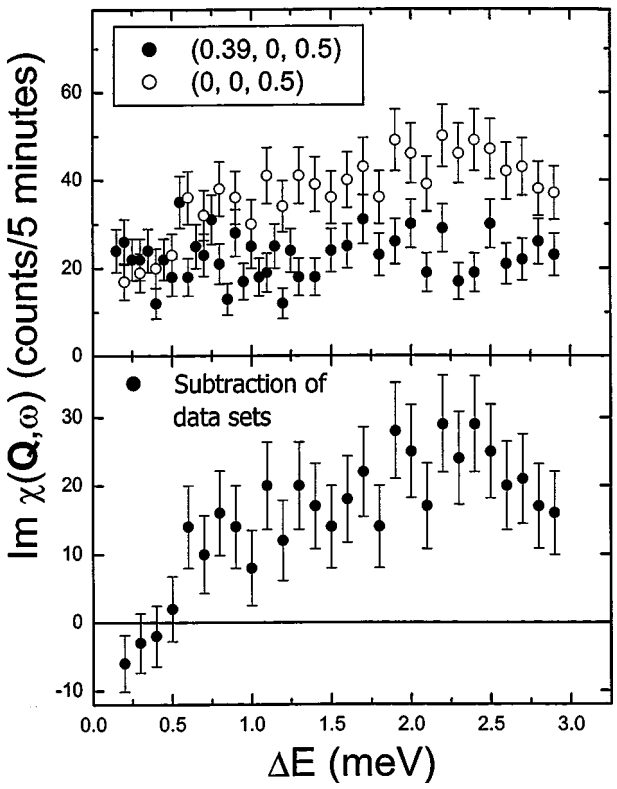

FIG. 9. Im $\chi(\mathbf{Q},\omega)$, derived from high energy resolution measurements taken on SPINS at NIST, for $\mathbf{Q}=(0.39, 0, 0.5)$ an incommensurate ordering wave vector, as well as $\mathbf{Q}=(0, 0, 0.5)$, the commensurate wave vector which describes magnetic order in UPd_2Al_3, is shown at $T=1.4$. The top panel shows the individual data sets, while the bottom panel shows their difference. Clearly the spectral weight moves from the commensurate wave vector (0, 0, 0.5) to the incommensurate wave vector (0.39, 0, 0.5) on the energy scale of 0.5 meV$\sim T_N$.

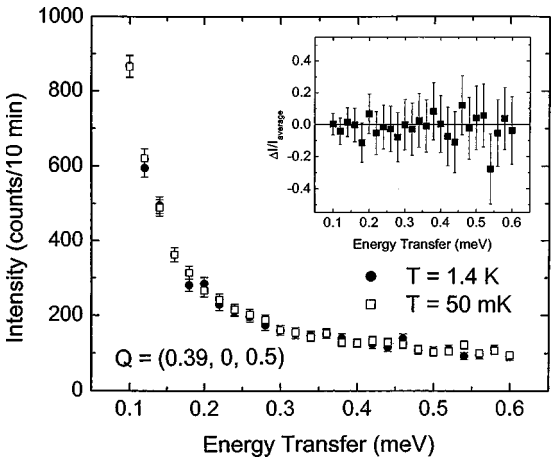

FIG. 10. Constant-**Q** scans at the incommensurate ordering wave vector (0.39, 0, 0.5), and very high energy resolution taken with SPINS at NIST is shown for temperatures above ($T=1.4$ K) and below ($T=0.05$ K) the superconducting phase transition ($T_C=1.2$ K). The difference between the two scans is shown in the inset to the figure. These data show that to within the ~3% accuracy of the measurement, no change in magnetic inelastic intensity is observed at the ordering wave vector in UNi_2Al_3 as the superconducting phase is entered, in contrast to its sister heavy fermion superconductor, UPd_2Al_3.

of these two data sets is shown in the lower panel. Clearly the magnetic inelastic scattering at the commensurate wave vector dominates, but only for energies above ~0.4 meV which is T_N. Consequently we conclude that the dynamic fluctuations in both UNi_2Al_3 and UPd_2Al_3 are indeed very similar, and the differences which underlie their disparate ordered structures only manifest themselves on energy scales associated with T_N itself. Such a conclusion would *not* be derived from the constant-**Q** scans taken by Aso *et al.*,[21] whose 0.2-K data show the scattering at the commensurate wave vector (0, 0, 0.5) to be less than that at either of the incommensurate ordering wave vectors (0.39, 0, 0.5) or (0.61, 0, 0.5) for all energies less than 1.5 meV~16 K.

Very high energy resolution measurements were performed using the SPINS spectrometer, 2.5-meV incident neutrons and a five crystal, horizontally-focused analyzer in order to obtain energy resolution ~0.1 meV (FWHM). This energy resolution is on a scale with T_C itself, and well below the characteristic energy scale associated with a BCS superconducting gap ($3.5k_BT_C$). Figure 10 shows constant-**Q** scans taken at the incommensurate ordering wave vector (0.39, 0, 0.5) at temperatures of 1.4 and 0.05 K, above and well below T_C, respectively. The difference in intensity at these two temperatures divided by the intensity itself is shown as a function of energy in the inset to Fig. 10. Clearly, to within the sensitivity of the present measurement, ~3% in intensity at energies above 0.1 meV, there is no change in the low-lying magnetic inelastic scattering near the ordering wave vector in UNi_2Al_3, as the superconducting state is entered.

This result is very different from the remarkable observation of a gapped magnetic excitation at the commensurate (0, 0, 0.5) ordering wave vector in UPd_2Al_3, which turns on below T_C.[22,23] Such an excitation may be qualitatively different within an incommensurate ordered structure as in UNi_2Al_3. In addition it may naively be expected to be harder to observe in UNi_2Al_3 than UPd_2Al_3, as the size of the average ordered moment is roughly six times smaller. In addition, no propagating spin waves are observed in UNi_2Al_3 at any wave vector. Still, the absence of clear changes in the magnetic fluctuations associated with the onset of superconductivity in UNi_2Al_3 indicate that the strong coupling between the superconductivity and magnetic fluctuations observed in UPd_2Al_3 is not a universal feature of these heavy fermion metals.

MEASUREMENTS OF THE ACOUSTIC PHONONS

Constant-**Q** inelastic measurements were also performed to investigate the low lying, acoustic phonons in UNi_2Al_3. These measurements were performed at BNL in constant $\mathbf{k}_f$ mode with scattered neutrons of energy 14.7 meV and ~1.5 meV (FWHM) energy resolution. As we were interested in the low lying excitations in UNi_2Al_3, it was important to understand the phonon scattering, so that, at the least, we

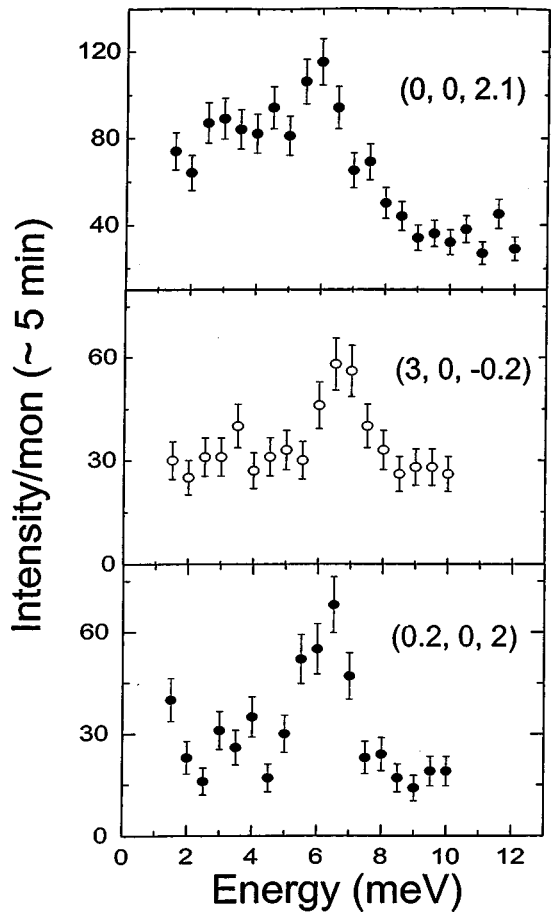

FIG. 11. Typical constant-**Q** inelastic scans which show a longitudinal acoustic (top panel) and two transverse acoustic phonon groups (middle and bottom panel). Their relevant dispersion is shown in Fig. 12.

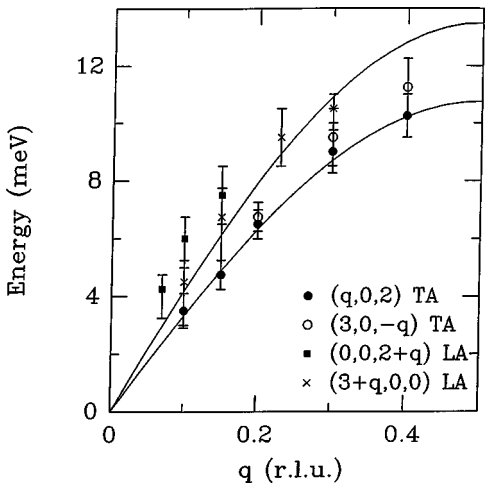

FIG. 12. The dispersion of the acoustic phonons, both longitudinal and transverse, propagating along both the **a*** and **c*** directions is shown. These results show that the low-lying acoustic phonons behave in a conventional manner, with zone boundary energies lying between 10 and 14 meV.

could be sure that the magnetic scattering was indentified cleanly.

Figure 11 shows representative constant-**Q** scans taken along $(0,0,2+q)$, $(3,0,-q)$, and $(q,0,2)$, where q denotes the propagation wave vector of the acoustic phonon in question. The $(\epsilon\cdot\mathbf{Q})^2$ part of the inelastic neutron scattering crosssection from phonons,[24] ensures that these wave vectors measure principally longitudinal acoustic branches and the two transverse acoustic branches, respectively. These measurements show the low lying acoustic phonons to be rather conventional. In Fig. 12, the energies associated with constant-**Q** scans shown in Fig. 11 are plotted as a function of the phonon propagation wave vector q, and these results were fitted to a simple sine wave dispersion relation. As can be seen, zone boundary acoustic phonon energies range from 10 to 13 meV, with the transverse modes consistently below the longitudinal modes in energy.

CONCLUSIONS

Inelastic neutron scattering measurements on UNi_2Al_3 have shown that the spectral weight of the spin fluctuations moves from the incommensurate antiferromagnetic ordering wave vectors $(\frac{1}{2}\pm\tau, 0, \frac{1}{2})$ with $\tau=0.11$ to the commensurate ordering wave vector $(0, 0, \frac{1}{2})$ as the energy of the fluctuations exceeds the energy scale of $T_N\sim 0.5$ meV. This observation is important as it accounts for one of the differences between UNi_2Al_3 and its quasi-isoelectronic, sister intermetallic, UPd_2Al_3, the difference in antiferromagnetic structures.

No propagating spin wave excitations are observed in UNi_2Al_3. The spectrum is quasielastic at all wave vectors studied, and has an energy width of roughly 6 meV, which correlated well with its coherence temperature of ~80 K. At low temperatures this scattering is peaked up around $(0,0,n/2)$, with n odd, and in ridges of the form $(H,0,0.5)$. On warming, this **Q** structure disappears, not by the peaks and ridges diminishing in intensity, but rather by the scattering between these features increasing in strength. The **Q** structure in the scattering is largely gone by the coherence temperature, ~80 K.

Very high energy resolution measurements investigated possible modifications to the magnetic fluctuations as the material became superconducting, as have been observed in UPd_2Al_3. To within a tolerance of ~3% in the intensity at the ordering wave vector, no such changes were observed for energies above 0.1 meV. Finally, the low lying acoustic phonons were investigated and found to behave rather conventionally, with zone boundary energies lying in the range from 10 to 14 meV.

ACKNOWLEDGMENTS

The support of all of our sponsors is gratefully acknowledged. This work was supported in part by NSERC of Canada. The work at Brookhaven National Laboratory was supported by the U.S. DOE, Division of Materials Sciences and Engineering, under contract No. DE-AC02-98-CH10886. Work at Johns Hopkins University was supported by the NSF through DMR0074571. Work at SPINS was based upon activities supported by the NSF under agreement No. DMR-9986442.

[1] Reviews of this topic can be found in N. Grewe and F. Steglich, in *Handbook on the Physics and Chemistry of Rare Earths*, edited by K. A. Gshneider, Jr. and L. Eyring (Elsevier, New York, 1991), Vol. 14, Chap. 97, p. 343; A. de Visser and J. J. M. Franse, J. Magn. Magn. Mater. **100**, 204 (1991); G. Aeppli and C. Broholm, in *Handbook on the Physics and Chemistry of Rare Earths*, edited by K. A. Gshneider, Jr. and L. Eyring (Elsevier, New York, 1994), Vol. 19, Chap. 131, p. 123; R. H. Heffner and M. R. Norman, Comments Condens. Matter Phys. **17**, 361 (1996).

[2] G. Aeppli, E. Bucher, C. Broholm, J. K. Kjems, J. Baumann, and J. Hufnagl, Phys. Rev. Lett. **60**, 615 (1985).

[3] K. Hasselbach, L. Taillefer, and J. Flouquet, Phys. Rev. Lett. **63**, 93 (1989).

[4] S. M. Hayden, L. Taillefer, C. Vettier, and J. Flouquet, Phys. Rev. B **46**, 8675 (1992), M. Boukhny, G. L. Bullock, B. S. Shivaram, and D. G. Hinks, Phys. Rev. Lett. **73**, 1707 (1994).

[5] T. T. M. Palstra, A. A. Menovsky, J. van der Berg, A. J. Dirkmaat, P. H. Kes, G. J. Nieuwenhuys, and J. A. Mydosh, Phys. Rev. Lett. **55**, 2727 (1985).

[6] C. Broholm, J. K. Kjems, W. J. L. Buyers, P. Matthews, T. T. M. Palstra, A. A. Menovsky, and J. A. Mydosh, Phys. Rev. Lett. **58**, 1467 (1987); C. Broholm, H. Lin, P. T. Matthews, T. E. Mason, W. J. L. Buyers, M. F. Collins, A. A. Menovsky, J. A. Mydosh, and J. K. Kjems, Phys. Rev. B **43**, 12 809 (1991).

[7] E. D. Isaacs, D. B. McWhan, R. N. Kleiman, D. J. Bishop, G. E. Ice, P. Zschack, B. D. Gaulin, T. E. Mason, J. D. Garrett, and W. J. L. Buyers, Phys. Rev. Lett. **65**, 3185 (1990); T. E. Mason, B. D. Gaulin, J. D. Garrett, Z. Tun, W. J. L. Buyers, and E. D. Isaacs, *ibid.* **65**, 3189 (1990).

[8] C. Geibel, C. Schank, S. Thies, H. Kitazawa, C. D. Bredl, A. Böhm, M. Rau, A. Grauel, R. Casparay, R. Helfrich, U. Ahlheim, G. Weber, and F. Steglich, Z. Phys. B: Condens. Matter **84**, 1 (1991).

[9] A. Krimmel, P. Fischer, B. Roessli, H. Maletta, C. Geibel, C. Schank, A. Grauel, A. Loidl, and F. Stegich, Z. Phys. B: Condens. Matter **86**, 161 (1992).

[10] T. Petersen, T. E. Mason, G. Aeppli, A. P. Ramirez, E. Bucher, and R. N. Kleiman, Physica B **199–200**, 151 (1994); T. E. Mason, T. Petersen, G. Aeppli, W. J. L. Buyers, E. Bucher, J. D. Garrett, K. N. Clausen, and A. A. Menovsky, *ibid.* **213–214**, 11 (1995).

[11] B. D. Gaulin, D. Gibbs, E. D. Isaacs, J. G. Lussier, J. N. Reimers, A. Schröder, L. Taillefer, and P. Zschack, Phys. Rev. Lett. **73**, 890 (1994).

[12] C. Geibel, S. Thies, D. Kaczororowski, A. Mehner, A. Grauel, B. Seidel, U. Ahlheim, R. Helfrich, K. Petersen, C. D. Bredl, and F. Steglich, Z. Phys. B: Condens. Matter **83**, 305 (1991).

[13] A. Schröder, J. G. Lussier, B. D. Gaulin, J. D. Garrett, W. J. L. Buyers, L. Rebelsky, and S. M. Shapiro, Phys. Rev. Lett. **72**, 136 (1994); J. G. Lussier, A. Schröder, B. D. Gaulin, J. D. Garrett, W. J. L. Buyers, L. Rebelsky, and S. M. Shapiro, Physica B **199–200**, 137 (1994).

[14] J. G. Lussier, M. Mao, A. Schroeder, J. D. Garrett, B. D. Gaulin, S. M. Shapiro, and W. J. L. Buyers, Phys. Rev. B **56**, 11 749 (1997).

[15] S. Sullow, B. Becker, A. de Visser, M. Mihalik, G. J. Nieuwenhuys, A. A. Menovsky, and J. A. Mydosh, J. Phys.: Condens. Matter **9**, 913 (1997).

[16] V. Barzykin and L. P. Gor'kov, Phys. Rev. Lett. **70**, 2479 (1993).

[17] M. B. Walker, W. J. L. Buyers, Z. Tun, W. Que, A. A. Menovsky, and J. D. Garrett, Phys. Rev. Lett. **71**, 2630 (1993); W. J. L. Buyers, Physica B **223–224**, 9 (1994).

[18] K. Matsuda, Y. Kohori, T. Kohara, K. Kuwahara, and H. Amitsuka, Phys. Rev. Lett. **87**, 087203 (2001).

[19] O. O. Bernal, C. Rodrigues, A. Martinez, H. G. Lukefahr, D. E. MacLaughlin, A. A. Menovsky, and J. A. Mydosh, Phys. Rev. Lett. **87**, 196402 (2001).

[20] See, for example, A. C. Hewson, *The Kondo Problem to Heavy Fermions* (Cambridge University Press, Cambridge, 1993).

[21] N. Aso, B. Roessli, N. Berhoeft, R. Calemczuk, N. K. Sato, Y. Endoh, T. Komatsubara, A. Hiess, G. H. Lander, and H. Kadowaki, Phys. Rev. B **61**, R11 867 (2000).

[22] N. Metoki, Y. Haga, Y. Koike, and Y. Omuki, Phys. Rev. Lett. **80**, 5417 (1998).

[23] N. Bernhoeft, N. Sato, B. Roessli, N. Aso, A. Hiess, G. H. Lander, Y. Endoh, and T. Komatsubara, Phys. Rev. Lett. **81**, 4244 (1998).

[24] S. W. Lovesey, *Theory of Neutron Scattering From Condensed Matter* (Clarendon Press, Oxford, 1984), Vol. 2.